Chemico-Biological Interactions 360 (2022) 109950

Contents lists available at ScienceDirect

Chemico-Biological Interactions

journal homepage: www.elsevier.com/locate/chembioint

Research paper

Biochemical changes in cancer cells induced by photoactive nanosystem based on carbon dots loaded with Ru-complex

Maja D. Nešić [a,*], Tanja Dučić [b], Mara Gonçalves [c], Milutin Stepić [a], Manuel Algarra [d,**], Juan Soto [e], Branislava Gemović [f], Teresa J. Bandosz [g], Marijana Petković [a]

[a] Center for Light-based Research and Technology COHERENCE, Department of Atomic Physics, Vinča Institute of Nuclear Sciences, National Institute of the Republic of Serbia, University of Belgrade, Belgrade, Serbia
[b] ALBA-CELLS Synchrotron, MIRAS Beamline, Cerdanyola Del Vallès, Barcelona, Spain
[c] CQM-Madeira Chemistry Research Centre, University of Madeira, Funchal, Portugal
[d] INAMAT^2 - Institute for Advanced Materials and Mathematics, Public University of Navarre, Campus de Arrosadia, 31006, Pamplona, Spain
[e] Department of Physical Chemistry, Faculty of Science, University of Málaga, Málaga, Spain
[f] Laboratory for Bioinformatics and Computational Chemistry, Vinča Institute of Nuclear Sciences, National Institute of the Republic of Serbia, University of Belgrade, Belgrade, Serbia
[g] Department of Chemistry and Biochemistry, The City College of New York, 160 Convent Ave, NY, 10031, USA

ARTICLE INFO

Keywords:
Anticancer photodynamic therapy
Biochemical changes
N-doped carbon dots
Carbon dots
Ru-metallodrug

ABSTRACT

Carbon dots (CDs) and N-carbon dots (N-CDs) loaded with Ru-complex (CDs@RuCN, N-CDs@RuCN, respectively) were investigated as media imposing biochemical changes induced by UV illumination of ovarian cancer, A2780, and osteosarcoma, CAL72, cells. Synchrotron radiation-based Fourier Transform Infrared Spectroscopy was performed, and the spectra were subjected to a Principal Component Analysis. The CDs@RuCN and N-CDs@RuCN effects on cancer cells were analyzed by the theoretical modelling of the stability of the composite systems and a protein database search. Moreover, a detailed evaluation of surface and optical properties of CDs@RuCN and N-CDs@RuCN was carried out. Results demonstrated selective action of the CDs@RuCN and N-CDs@RuCN-based photodynamic therapy, with N-CDs@RuCN being the most active in inducing changes in A2780 and CDs@RuCN in CAL72 cells. We assume that different surface charges of nanoparticles led to direct interactions of N-CDs@RuCN with a Wnt signalling pathway in A2780 and those of CDs@RuCN with PI3–K/Akt in CAL72 cells and that further biochemical changes occurred upon light illumination.

1. Introduction

Carbon dots (CDs) are low-cost, water-soluble, nanosized light harvesters with high efficiency to generate reactive oxygen species (ROS). These features might direct their potential application as photosensitizers (PSs) in photodynamic therapy (PDT) [1,2]. CDs have been reported to efficiently suppress cancer cell growth *in vitro*, such as Hep G2 liver cancer cells, by triggering oxidative stress and damaging vital cellular biomolecules [3,4]. Similar inhibition has been observed in breast cancer cell lines (MDA-MB-231 and MCF-7), in which CDs caused the generation of a large amount of ROS [3]. Published results indicated that doping of CDs with heteroatoms, such as N, S or B, can enhance their light absorption capability and improve their quantum yield, important for the oxygen photosensitization essential for the application in PDT [5,6]. Furthermore, the surface of CDs can be easily functionalized with drugs, which have rapid renal clearance, resulting in CDs -nano-based drug carriers [7,8].

Nano-based drug carriers are intended to arrive at the tumor sites owing to their enhanced permeability and retention effect [9]. Nevertheless, as many other nanomaterials developed, most CDs reported to date are mainly localized in the organelles in the cytoplasm, *i.e.* the lysosomes, mitochondria, Golgi apparatus and endoplasmic reticulum [10,11]. To further enhance PDT, CDs need to be functionalized to enter a cell nucleus, which is an optimal site for cancer treatment. When CDs reach the nucleus, the attached drug can be released and damage the genes to stop the proliferation of the cancer cell without being trapped or neutralized in the cell cytoplasm [12]. CDs contain an sp^2/sp^3 hybridized carbon structure that can attract aromatic-ring drugs via strong π-π interactions. In this study, CDs were modified with a Ru-complex

* Corresponding author.
** Corresponding author.
E-mail addresses: maki@vin.bg.ac.rs (M.D. Nešić), manuel.algarra@unavarra.es (M. Algarra).

https://doi.org/10.1016/j.cbi.2022.109950
Received 4 January 2022; Received in revised form 1 April 2022; Accepted 11 April 2022
Available online 14 April 2022

Abbreviations

CDs	Non-doped carbon dots
N-CDs	Nitrogen-doped carbon dots
RuCN	(η^5-cyclopentadienyl)bis(triphenylphosphine) ruthenium(II), (Ru(η^5-C_5H_5)(PPh_3)$_2$CN)
CDs@RuCN	Non-doped carbon dots loaded with (Ru(η^5-C_5H_5)(PPh_3)$_2$CN)
N-CDs@RuCN	Nitrogen-doped carbon dots loaded with (Ru(η^5-C_5H_5)(PPh_3)$_2$CN)
A2780	ovarian cancer cell line
CAL72	osteosarcoma cancer cell line
SR-FTIR spectroscopy	Synchrotron Radiation-based Fourier Transform Infrared Spectroscopy
PSs	photosensitizers
PDT	photodynamic therapy
NPs	nanoparticles

containing aromatic ligands to create a nanocomposite system that can interact with intracellular biomolecules and potentially reach the cell nucleus. Upon light illumination, certain Ru-complexes can generate singlet molecular oxygen and/or undergo ligand dissociation, which can result in coordination of the Ru fragment with DNA or proteins, thus enhancing the cytotoxicity [13,14]. Non-doped and N-doped CDs loaded with cyano (η^5-cyclopentadienyl) bis (triphenylphosphine) ruthenium (II) (Ru(η^5-C_5H_5)(PPh_3)$_2$CN) (RuCN complex, further in the text) (CDs@RuCN and N-CDs@RuCN, respectively) are tested as photosensing agents in PDT of osteosarcoma and human ovarian cancer (CAL72 and A2780 cancer cell lines, respectively). Our objective is to evaluate the effect of CDs' properties on the capability of the composites to impose changes in the structure of cellular biomolecules in the dark and upon UV illumination, and thus to be used in PDT. We also intend to isolate the effect of light to elucidate the contribution of these photosensitizers (PSs) to the biochemical processes triggered by the illumination. To our knowledge, there is only one study of biochemical changes in cells during PDT, in which the cumulative effects of photosensitizer, Hypocrellin A, and the light were observed by SR FTIR [15]. Based on recorded structural changes in lipids, proteins, and nucleic acids in A2780 and CAL72 cells initiated by the illumination, we evaluated the effects of CDs composites' surface chemistry on the complexity of the PDT mechanism in different cancer cell types. Finally, potential target proteins belonging to specific signalling pathways are theoretically identified as affected by the CDs photoactivity.

2. Material and methods

2.1. Synthesis of Ru complex and CDs

The synthesis of RuCN, cyano (η^5-cyclopentadienyl) bis (triphenylphosphine) ruthenium (II) (Ru(η^5-C_5H_5)(PPh_3)$_2$CN), was carried out following the methodology reported previously, with some modifications [16]. CDs were obtained from lactose (1 M) by hydrothermal treatment at 120 °C for 3 h, as previously reported by our group [17]. CDs enriched with nitrogen (N-CDs) were obtained by exposing the previously obtained CDs to 1,6-hexane diamine for 3 h at 100 °C. This method showed good reproducibility of the synthesis procedure, demonstrated by the results of XPS analysis [18,19]. Based on these results, the chemistry of synthesized nanocarbons used in this study, along with that of ruthenium complex, is shown in Table S2.

2.2. Cell cytotoxicity assay

Cells were grown in RPMI 1640 (A2780) or DMEM (CAL72) medium containing 10% serum and 1% antibiotics and supplemented with other essential ingredients. Afterwards, cells were harvested, cultured at a density of 10 000 cells/well and incubated with various concentrations of RuCN (concentration range 2.5–20 μM) or with CDs/N-CDs (20 μg - 0.5 mg/mL), Fig. S1, for 2 h prior to illumination with a UV lamp (60 μW, 350 nm, 10 min). The cytotoxicity was evaluated after 48 h exposure by measuring the metabolic activity of cells using the Resazurin reduction assay, according to the vendor's instructions. Non-treated cells were used as controls.

2.3. Preparation of cells for SR-FTIR spectroscopy

Cell cultures of A2780 and CAL72 were grown in an incubator at 37 °C, with 5% CO_2 atmosphere on a round 10 × 0.5 mm^2 CaF_2 carrier (minimum 60 000 cells/sample) and treated with 12.5 μM RuCN containing 20 μg/mL either CDs or N-CDs before the SR FTIR spectroscopy. After 24 h of incubation, cells were washed twice with PBS and lyophilized in a Martin Christ Freeze-dryer Alpha lyophilizer 1–2 Labconco Freeze Zone 4.5 L Freeze Drier Systems (Germany). The conditions of lyophilization were as follows: the temperature of −50 °C, the vacuum of 0.3 mBa for 24 h. Samples were stored over silica gel before the SR-FTIR spectroscopy data acquisition.

2.4. Synchrotron radiation Fourier transform infrared (SR FTIR) spectroscopy

Intracellular changes in biomolecules were analyzed by the SR-FTIR spectroscopy (Synchrotron ALBA, MIRAS beamline, Barcelona, Spain) [20], and technical details were the same as described previously [21]. The aperture of the FTIR microscope was set to a size of a single cell (12 × 12 μm^2), and 60 cells were analyzed from each group. In total, three independent replicates were analyzed with co-adding 256 spectra at 4 cm^{-1} resolution.

2.5. Data processing and statistical evaluation

For comparisons between different regions and bands, averaged spectra were analyzed after a baseline correction and vector normalization. SR FTIR spectra were processed by using the Orange Spectroscopy tools [22], which allows multimodal spectral analysis involving PCA. The bands with the highest differences in position and intensity were identified as outliers (maximum three per sample) and excluded from further calculations. From the spectra, the intensity of the C═O band and the CH_2/CH_3 ratio were calculated and compared within different groups of samples by using the Analysis of Variance (ANOVA) test.

3. Theory/calculation

3.1. Bioinformatics analysis

To identify potential protein targets of CDs that are specific for A2780 and CAL72 cell lines, we used the baseline gene expression in these cell lines and the comparison between them. The Expression Atlas [23], a freely available resource of the European Bioinformatics Institute for the gene expression across species, was browsed. The genes with abundant expression in each of the cell lines, which are not expressed in the other cell line, were further analyzed using the DAVID enrichment tool [24]. The enrichment analysis was based on the comparison between the number of genes in the input list annotated with the specific term and the number of genes annotated with the same term in the whole genome. DAVID uses modified Fisher's Exact test to measure gene enrichment in annotation terms. For the annotation of analyzed proteins, we selected Kyoto Encyclopedia of Genes and Genomes (KEGG) pathways [25]. We browsed PDBsum [26], a publicly available pictorial database of protein 3D structures, in search of the 3D structures of

proteins identified as the potential targets of CDs/NCDs. PDBsum was searched by a protein sequence, which was downloaded, as a canonical protein isoform, from an UniProt database (The UniProt Consortium, 2019).

3.2. Density functional theory (DFT) calculations

The calculations of surface and optical properties of CDs@RuCN and N-CDs@RuCN were performed with the density functional theory (DFT) by applying the M05-2X function [27] with the empirical dispersion correction of Grimme [28] and the def2-SVPP, and def2-TZVPP basis sets [29] as they are implemented in the Gaussian program. This methodology has been already successfully applied to an analogous Ru-complex [30].

4. Results and discussion

4.1. Cytotoxic and UV light photo-cytotoxic activity of CDs, N-CDs and Ru-complex

The metabolic activity was observed upon the treatment of A2780 and CAL72 cells with CDs, N-CDs and RuCN in the dark (Fig. 1A) or upon light illumination (Fig. 1B). The treatment of A2780 cells with CDs did not result in significant cytotoxicity, whereas the incubation achieved a marked viability reduction with N-CDs and RuCN.

The illumination of A2780 cells treated with CDs and N-CDs seemed to recover their metabolic activity. In the case of the RuCN/light-treated cells, metabolic activity was lower compared to the non-treated illuminated cells. The treatment of CAL72 with CDs in the dark resulted in a significant decrease in cell metabolic activity (Fig. 1A), whereas the UV light increased cytotoxicity of all substances, *i.e.* CDs, N-CDs and RuCN (Fig. 1B).

Cells could become more metabolically active after treatment with nanoparticles (NPs), which is attributable to the activation of proliferation and growth pathways triggered by the adhesion of NPs to cells [31], but our findings agree with the findings of other authors [32], who reported the increased toxicity and apoptosis in the cells upon their interactions with CDs. We assume that observed diverse effects can be explained by the cell-line dependent signalling differences.

The enhanced effect of UV on cytotoxicity can be linked to the photoactivity of CDs/N-CDs upon UV illumination. In this process, ROS might be generated in the cells, which cause cellular damage and, consequently, cell death. In addition, RuCN also demonstrated a photosensitizing effect after UV irradiation (Fig. 1B), which is observed as a decrease in metabolic activity compared to the cell treatment in the dark. These results imply that both components of the system, CDs and RuCN, have the potential to act as photosensitizers, which is explored further.

4.2. The theoretical model of CD@RuCN and N-CD@RuCN as photosensitizers

As we already mentioned, both components of the system (RuCN and (N-)CDs) have been characterised previously and are photoactive in the UV region (Table S2). In order to enhance photoactivity, two components are combined. The surface and optical properties of CDs@RuCN and N-CDs@RuCN are of crucial importance to identify their potential biomolecular targets in A2780 and CAL72 cells and to explain their photosensitizing activity. Geometries are illustrated in Fig. 2, whereas theoretically obtained excitation/absorption of RuCN, CDs@RuCN and N-CDs@RuCN, enthalpies and Gibbs free energies of the reactions of formation of the drug-carrier complexes as well band gaps (vertical excitations) and oscillator strengths of the electronic transitions are presented in Table S1.

Calculations provided the following significant findings: a) the interaction of RuCN with both CDs and N-CDs is stable, with the CDs (COOH)@RuCN found to be the most favourable from both the energetic and dynamics viewpoints; b) results suggest that the complexes of CDs and N-CDs with RuCN will act as PS in augmenting the effect of light on the cells as the oscillator strengths of the UV active bands increase in passing from the Ru-complex to CDs@RuCN, N-CDs@RuCN (Table S1).

4.3. SR-FTIR spectroscopy study of biochemical changes in CAL72 and A2780

The extent and nature of biochemical changes in two cancer cells upon UV illumination in the presence of CDs@RuCN and N-CDs@RuCN were investigated by comparing SR FTIR spectra of illuminated cells with their treatment in the dark. As shown, both components of the system are expected to be photoactive and absorb in the UV range (Table S2), but their effect was cell line-dependent. We found that CDs@RuCN and N-CDs@RuCN act selectively in terms of induced biochemical changes in these two cell lines, and that selectivity is achieved by the differences in cellular mechanisms between various cancer types. Although it is assumed that the increased level of oxidative stress triggered by the light is responsible for the observed photokilling effect [33], the cellular response depends on the cell biomolecular composition mostly related to the signalling pathways. CDs@RuCN and N-CDs@RuCN are mediators for PDT, and their interaction with intracellular biomolecules may focus the action of light [34].

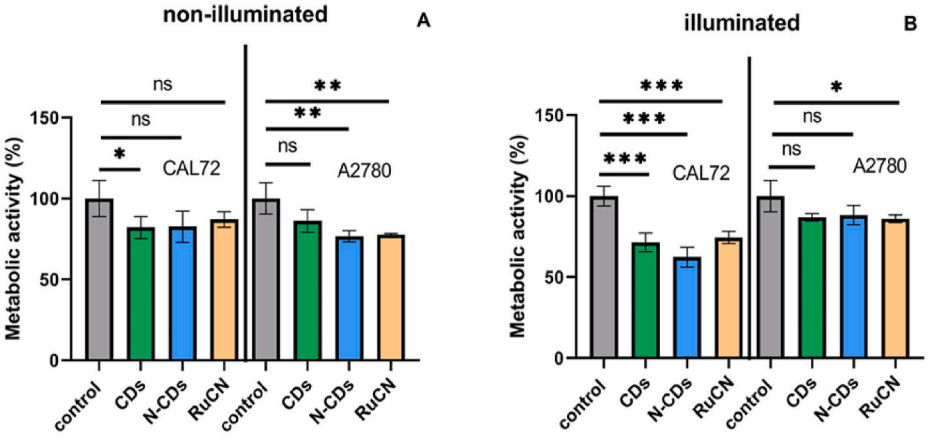

Fig. 1. Metabolic activity (%) of non-illuminated (A) and illuminated (B) CAL72 and A2780 cancer cell lines upon treatment with CDs, N-CDs, and RuCN. The metabolic activity of non-treated cells is set up as 100%, and cells are incubated with RuCN, CDs or N-CDs for 2 h directly before illumination. An asterisk indicates the significant differences in the viability (*$p < 0.05$, **$p < 0.01$, ***$p < 0.001$), and *ns* indicates a lack of statistically significant difference.

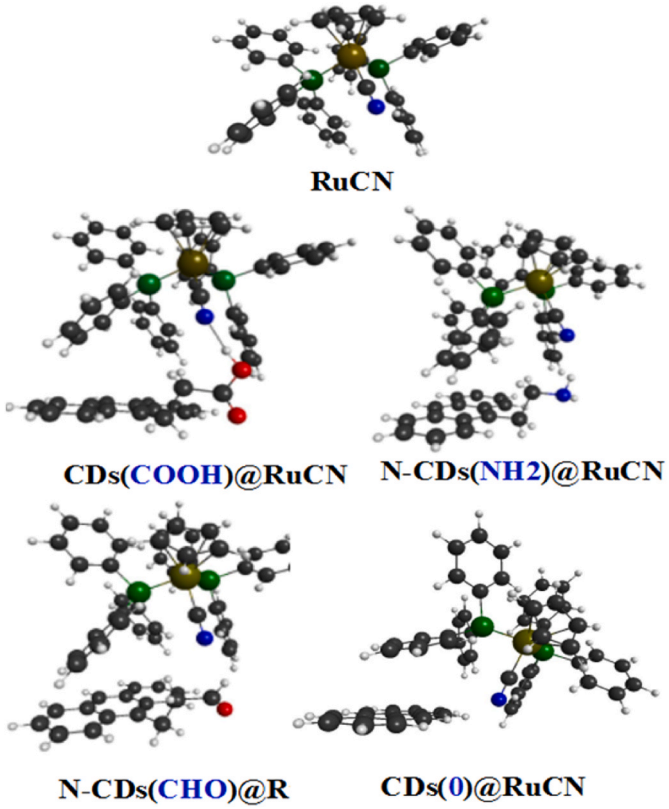

Fig. 2. Geometries of RuCN and models selected for CDs@RuCN and N-CDs@RuCN complexes.

The starting point of our approach is the treatment of the cells with CDs@RuCN and N-CDs@RuCN (Fig. 2) at a fixed concentration. The cells were treated in the dark or upon UV illumination, and the extent of changes induced by illumination was studied in detail by IR spectroscopy. Infrared spectra were divided into three regions that correspond to principal classes of biomolecules, processed and evaluated separately: **lipids** (~3050-2800 cm^{-1}), **proteins** (~1800-1480 cm^{-1}) and **nucleic acids** (NA) and **carbohydrates** (~1480-900 cm^{-1}). In the NA- and carbohydrate region, two bands were associated with changes in the lipids' structure: the band from ~1480 to 1430 cm^{-1} (linked to bending vibrations of unsaturated aliphatic chains) and ~1430-1360 cm^{-1} corresponds to vibrations of carboxylic acids and/or aldehydes [35,36]. A principal component analysis (PCA) was performed for each region. The second derivative of the spectral region corresponding to the Amide I bands was obtained in order to identify precisely differences between two groups of spectra and assign the changes in protein conformation, *i.e.* secondary structure, induced by CDs@RuCN or N-CDs@RuCN treatment and/or UV illumination. Since we hypothesize that the differences in signalling pathways, related to the chemistry of nanocarbon used, cause selectivity in response to PDT, we have first analyzed the changes in the protein region in both cells.

4.3.1. SR-FTIR spectroscopy analysis of protein changes

In the case of both cells, illumination causes significant changes in the protein spectral region. The most affected parts of the proteins in the Amide I and Amide II regions, together with the carbonyl and carboxyl groups in the area from 1480 cm^{-1} to 1800 cm^{-1}, are displayed in Fig. 3A and E for A278 and CAL72 cells, respectively. The Amide I band was analyzed in detail to visualize differences in various protein secondary structures, and the second derivative is shown in Fig. 3B and 2F (A2780 and CAL72, respectively). The second derivative showed a shift of the Amide I band (detected at ~ 1649 cm^{-1}-1651 cm^{-1}) to the maximum at ~1655 cm^{-1} after interaction with N-CDs@RuCN upon illumination. This band corresponds to the Amide I C═O stretching vibration, and its shift was observed after the bovine serum albumin (a protein) interactions with Ru-ion [37]. The band at ~ 1630 cm^{-1}, corresponding to the β-secondary structure, changed upon the treatments, especially for A2780 (an arrow in Fig. 3B).

The first component in the PCA showed the most prominent contribution of the broad band at ~1630 and 1553 cm^{-1}, and PC2 pointed out the differences in the protein conformation at ~1542 $cm^{-1}$and ~1648 cm^{-1} (minima of the plot, Fig. 3C) of the A2780 cells. These peaks are assigned to an α-helix and random coil structure, respectively. The corresponding signals are more pronounced in the CDs@RuCN/UV, and N-CDs@RuCN/UV treated cells (Fig. 3C) compared to non-illuminated ones. Maxima of the PC2 are the range of carbonyl and carboxyl groups (~1765 cm^{-1} and ~1734 cm^{-1}). These structures were the most pronounced in N-CDs@RuCN (green dots in Fig. 3D).

In CAL72 cells, the differences in the SR FTIR spectra are detectable in the Amide I band (Fig. 3E, an arrow in Fig. 3F). This is also confirmed by the PCA: the most pronounced differences were detected in the 1554 cm^{-1} band and broad band at ~1630 (PC1) (Fig. 3G, PC loadings). The minima of PC2 at ~1648 cm^{-1} are assigned to the random coil, and they are more pronounced in the UV-treated cells. The maxima in PC2 are at ~1567 cm^{-1}, and they could be assigned to amino acids residues and/or possibly aggregated β-sheet structures. Also, one of the PC2 maxima is at 1755 cm^{-1} and it corresponds to the ester groups [38,39]. The PC1 and PC2 scores show clearly different patterns after the various treatments (Fig. 3H), with the CDs@RuCN treatment being the most efficient in inducing protein changes in CAL72 cells.

Our data are consistent with the findings of Chio-Srichan and coworkers [15], who reported significant changes of the Amide I and II regions (changes in the secondary protein structure) in HeLa cells treated with PS, i.e. Hypocrellin A and upon light illumination. In our case, the extent of the proteins' conformal changes is the cell and CD-dependent: N-CDs@RuCN imposed more pronounced changes in A2780, and CDs@RuCN in the CAL72 cells. Additionally, changes in the α-helix are more visible upon illumination of A2780 cells than those in CAL72.

4.3.2. Bioinformatics analysis of potential target proteins in A2780 and CAL72 cells

Since UV illumination induces various changes in the protein structure depending on the cell line and the type of CDs used, the specificity of the proteins present in the tested cell lines and thus their interactions with nanocarbon based PS govern the observed behaviour. These proteins might be target molecules whose structural changes affect the individual cell viability upon tested conditions. To check this hypothesis, we have searched the Expression Atlas database and chose the expression results of experiments E-MTAB-2770 for A2780 and E-MTAB-3983 for CAL72 cell lines. There were 14807 and 13925 expressed genes, with the baseline expression ≥2.0 TPM (Transcripts Per Million), in these two cell lines, respectively. There were 3281 genes specifically expressed (≥2.0 TPM cut-off) in the A2780 cell line and 2398 genes specifically expressed in the CAL72 cell line. Subsets of these genes, with the expression ≥20 TPM, were selected for enrichment analysis with the DAVID tool. The most significantly enriched (Kyoto Encyclopedia of Genes and Genomes (KEGG) metabolic library in the A2780-specific subset of genes was a Wnt signalling pathway, including seven genes (Table 1). For three of these genes, a 3D structure of a part of the protein was resolved and overviewed in the PDBsum database (Table 2). Chains in proteins WIF1 and TP53 contain, among other secondary structure motifs, four and two β-sheets, respectively. These could be the structures affected with the treatment of A2780 cells with the N-CDs@RuCN, described in the previous section as a change in the peak at ~1635 cm^{-1}. Additionally, a protein chain with a resolved 3D structure of the protein CXXC4 encompasses four helices (Table 2), which could be the structures affected by the treatment of A2780 cells with both CDs@RuCN and N-CDs@RuCN (a change in the region ~1660 cm^{-1}-1655 cm^{-1} of the

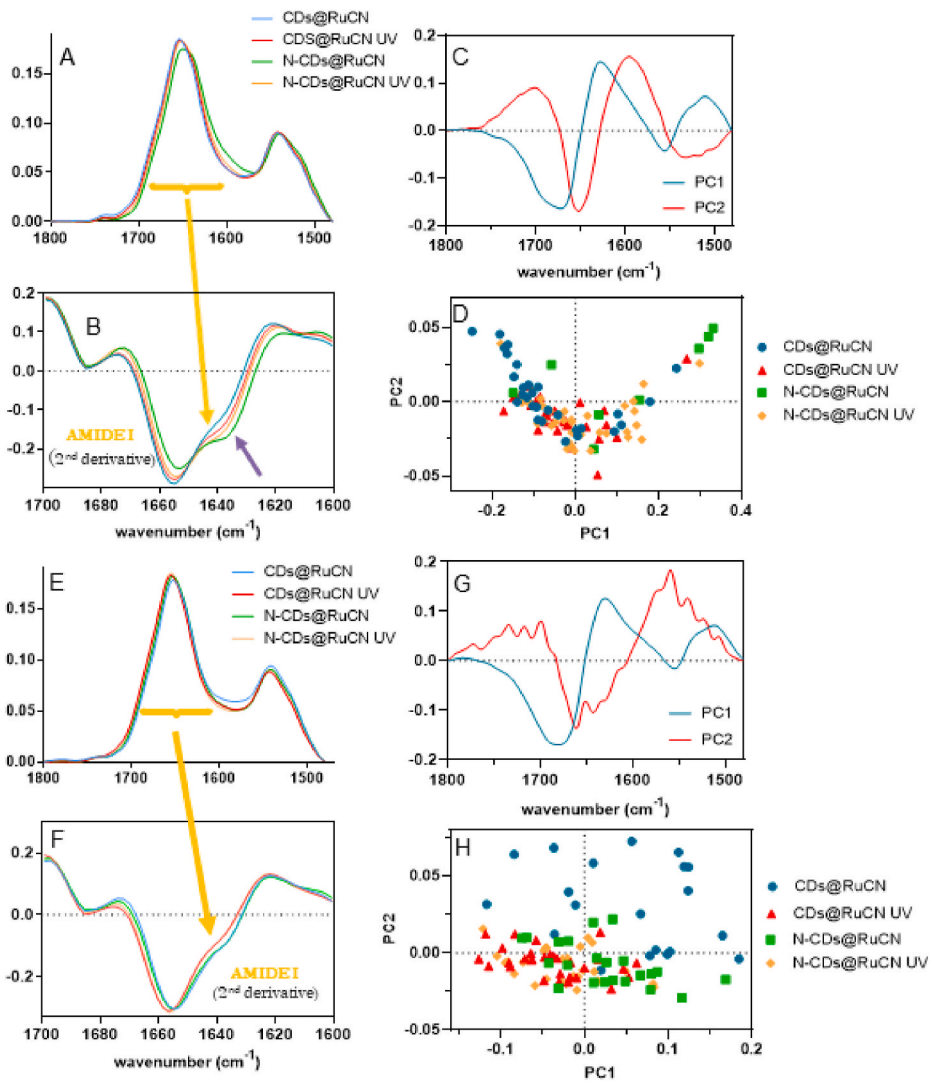

Fig. 3. SR-FTIR spectra (**A**, **E**) of the protein region and the second derivative of the Amide I regions (**B**, **F**) of A2780 and CAL72 cells, respectively, treated with CDs@RuCN and N-CDs@RuCN. In **C** and **G** the loadings for PC1 and PC2 are given, whereas in **D** and **H** the PC1 × PC2 graphs for A2780 and CAL72 cells, respectively, are presented. Blue lines in the spectra represent the cells treated with CDs@RuCN, and red ones represent the cells treated with CDs@RuCN and illuminated. The treatment with N-CDs@RuCN is represented by the green lines in both spectra, whereas the same treatment upon illumination is given in orange.

FTIR spectra). The Wnt//β-catenin pathway regulates cell proliferation and apoptosis, as well as a stem cell fate in embryonic and adult tissues [25]. This pathway was previously shown to be hyperactivated in ovarian cancers, although the underlying mechanisms are still elusive. Nevertheless, the inhibition of the Wnt/β-catenin pathway can have therapeutic potential, which is why it is already recognized as an important target for ovarian cancer therapy [26,27].

In the CAL72-specific subset of genes, the most significantly enriched KEGG pathway was phosphatidylinositol 3-kinase (PI3K)/Akt signalling pathway, encompassing 18 genes (Table 2). For 11 of these genes, PDBsum entries were overviewing the 3D structures of the chains in the corresponding proteins. Secondary structure motifs from eleven proteins, MET, CDK6, FGF1, FN1, ITGA2, ITGA4, IL7R, NGF, PRKCA, THEM4 and THBS2, include at least one sheet (Table 1).

This is consistent with the changes in the spectral region attributed to the β-sheet structures described in the previous section in CAL72 cells after the treatment with CDs@RuCN and N-CDs@RuCN. The (PI3K)/Akt pathway is one of the key pathways in human cancers, and it was shown to be hyperactivated in osteosarcomas [40]. It is involved in the majority of phases of initiation and progression of osteosarcomas, and therefore it is one of the most valuable targets in the treatment of these cancers [41,42]. Based on the above-mentioned results, the most probable proteins involved in the diverse effects of CDs@RuCN and N-CDs@RuCN under UV light are associated with the aforesaid signalling pathways.

4.3.3. SR-FTIR spectroscopy study of the changes in the lipid region

UV illumination does not induce significant changes in the lipid region in the A2780 cells treated with CDs@RuCN (Fig. 4A and B, blue and red lines and dots in PC1 x PC2 graphs, Fig. S2), whereas in the presence of N-CDs@RuCN (Fig. 4A and B) illumination leads to an increase in the intensity of CH_2-asymmetric and symmetric stretching bands (~2920 cm^{-1} and ~2850 cm^{-1}, respectively) (Figs. S2 and S3) [43]. A slight increase in the intensity of the CH_2 asymmetric stretching band might indicate an increased level of oxidative stress that affects cellular lipids upon light illumination [35], which is consistent with the implied PDT mechanism [33]. The carbonyl band corresponding to the C═O group has also moderately higher intensity in the case of N-CDs@RuCN treated and illuminated A2780 cells than the corresponding unilluminated analogue (Fig. S3A). These changes agree with detected changes in the cell metabolism (Fig. 1). Accordingly, the level of C═C band decreases, which is consistent with the increased level of oxidative stress (Fig. S2A). It is possible that N-CDs@RuCN interacts more readily with the membrane phospholipids, and therefore acts locally after the light illumination. The interaction of nanoparticles, or nanocomposite systems, with the cellular phospholipids and the cell membrane is a complex issue since it depends on the surface charge, shape and size of nanoparticles, as well as on the phospholipid composition and potential receptors on the cell surface [44]. However, since this also depends on the cell type, this hypothesis needs further experiments with the complex systems.

Table 1
Proteins involved in signalling pathways in **A2780** and **CAL72** cells were identified based on the analysis of the Expression Atlas database.

A2780 cells – Wnt signalling		
Gene symbol	Protein name	Expression (TPM)
CCND2	G1/S-specific cyclin-D2	537
CXXC4	CXXC-type zinc finger protein 4	215
TP53	Cellular tumor antigen p53	69
WIF1	Wnt inhibitory factor 1	54
VANGL2	Vang-like protein 2	41
APC2	Adenomatous polyposis coli protein 2	22
CER1	Cerberus	22
CAL72 – PI3K/Akt signalling		
Gene symbol	Protein name	Expression (TPM)
FN1	Fibronectin	362
THBS2	Thrombospondin-2	156
PRKCA	Protein kinase C alpha type	122
OSMR	Oncostatin-M-specific receptor subunit beta	94
GNG11	Guanine nucleotide-binding protein G(I)/G(S)/G (O) subunit gamma-11	89
LAMB1	Laminin subunit beta-1	76
AKT3	RAC-gamma serine/threonine-protein kinase	61
MET	Hepatocyte growth factor receptor	61
NGF	Beta-nerve growth factor	51
IL7R	Interleukin-7 receptor subunit Alpha	47
LPAR1	Lysophosphatidic acid receptor 1	46
PDGFC	Platelet-derived growth factor C	32
CDK6	Cyclin-dependent kinase 6	26
LAMA4	Laminin subunit alpha-4	26
FGF1	Fibroblast growth factor 1	25
ITGA2	Integrin alpha-2	24
ITGA4	Integrin alpha-4	22
THEM4	Acyl-coenzyme A thioesterase THEM4	21

Table 2
Secondary structures in proteins identified as possible targets of CDs.[a]

Protein	PDBsum ID	AA number	Secondary structures
CXXC4	5vc9	46	4 helices, 1 helix-helix interact, 4 beta turns
WIF1	2ygq	241	6 sheets, 6 beta hairpins, 5 beta bulges, 18 strands, 3 helices, 27 beta turns, 2 gamma turns, 10 disulphides
TP53	2fej	204	2 sheets, 3 beta hairpins, 4 beta bulges, 11 strands, 3 helices, 26 beta turns, 1 gamma turn
MET	6gcu	675	14 sheets, 28 beta hairpins, 23 beta bulges, 55 strands, 9 helices, 82 beta turns, 10 gamma turns, 10 disulphides
CDK6	1blx	305	2 sheets, 4 beta hairpins, 6 beta bulges, 7 strands, 15 helices, 13 helix-helix interacs, 17 beta turns, 2 gamma turns
FGF1	1ry7	151	5 sheets, 4 beta hairpins, 4 beta bulges, 12 strands, 4 helices, 23 beta turns, 4 gamma turns
FN1	3t1w	368	8 sheets, 12 beta hairpins, 10 beta bulges, 32 strands, 1 helix, 32 beta turns, 3 gamma turns
ITGA2	1aox	201	1 sheet, 3 beta alpha beta units, 1 beta hairpin, 1 beta bulge, 6 strands, 11 helices, 10 helix-helix interacs, 13 beta turns, 3 gamma turns, 1 disulphide
ITGA4	3v4v	582	11 sheets, 19 beta hairpins, 11 beta bulges, 40 strands, 6 helices, 76 beta turns, 14 gamma turns, 6 disulphides
IL7R	3up1	201	4 sheets, 7 beta hairpins, 4 beta bulges, 15 strands, 4 helices, 18 beta turns, 3 gamma turns, 3 disulphides
NGF	5jz7	110	4 sheets, 3 beta hairpins, 4 beta bulges, 9 strands, 13 beta turns, 3 gamma turns, 3 disulphides
PRKCA	3iw4	332	2 sheets, 5 beta hairpins, 5 beta bulges, 8 strands, 16 helices, 20 helix-helix interacs, 23 beta turns, 2 gamma turns
THEM4	4gah	172	1 sheet, 4 beta hairpins, 4 beta bulges, 7 strands, 4 helices, 1 helix-helix interact, 14 beta turns
THBS2	1yo8	621	8 sheets, 10 beta hairpins, 8 beta bulges, 28 strands, 11 helices, 94 beta turns, 7 gamma turns, 18 disulphides

[a] Data are retrieved from PDBsum. Only the proteins for which the information could be found are given in the table. AA-amino acids.

The analysis of the IR spectra of the lipid area in CAL72 cells showed that the signal at ~3014 cm^{-1} that arises from unsaturated C═C bonds [43] decreased significantly upon UV light illumination (Fig. 4B). This decrease in the intensity is more pronounced in the cells treated with CDs@RuCN compared to N-CDs@RuCN (Fig. 3A), and it indicates a reduction in the concentration of unsaturated bonds. These changes might be caused by the peroxidation of lipids, and based on the obtained results, it is possible that CDs@RuCN is more active than its N-doped analogue. A higher peroxidation activity in cells is also confirmed by the significantly changed CH_2/CH_3 ratio of asymmetric vibrations areas (Fig. S3B). Biochemical changes in the lipids-related signals of both cell lines upon light illumination were also detected in the spectral region from ~1480 to 1430 cm^{-1} (bending vibrations of unsaturated aliphatic chains) and from ~1430 to 1360 cm^{-1} that corresponds to vibrations of carboxylic acids and/or aldehydes [35,36] (*Cf.* further in the text).

In the spectra of CDs@RuCN-treated A2780 cells, the signal from ~1480 to 1430 cm^{-1} decreased upon illumination, and for CAL72 it increased. The band's intensity that corresponds to the carbonyl C═O group (1730-1760 cm^{-1}) increased relative to the total lipid bands in the A2780 cells (Fig. S3A) that are treated with N-CDs@RuCN and illuminated compared to unilluminated analogue. While the difference between various treatments is significant in this cell line, the increase in the C═O signal in the CAL72 cells is not statistically significant.

All changes detected in the lipid region of the spectra of the A2780 and CAL72 cells indicate different responses in these two types of cells. The decrease of C═C bands content, increase in carbonyl groups' signal and in the ratio of their peak areas to those of total lipids indicate advanced oxidative processes in the A2780, and in CAL72 cells, the extent of oxidation of unsaturated lipids increased upon illumination [33,45]. Besides, a shift of the bands corresponding to the CH_3 (asymmetric and symmetric) and CH_2 asymmetric vibrations towards higher wavenumbers might indicate the interactions between CDs@RuCN and the lipids of CAL72 cells, the hydrogen bond rearrangements caused by the light illumination, and consequently changes in membrane fluidity [46]. They can be triggered either by the oxidative modification of lipids or lipids fluidity changes [47], caused by ROS, initiated by the light catalyzed by CDs@RuCN and N-CDs@RuCN. Also, the photosubstitution reactions, to which RuCN is susceptible [48], can play a role in indicated changes. Although detectable, the differences in the lipid region induced by the illumination of the A2780 cells are not statistically significant, as shown by PCA, whereas, in the CAL72 cells, these changes are more obvious (Figs. S2 and S3).

4.3.4. *SR-FTIR spectroscopy study of changes in the nucleic acid region*

The most significant changes in the IR spectra of the cells are observed in the signals at ~1240 cm^{-1} and 1080 cm^{-1}, corresponding to the phosphodiester bands of NAs (asymmetric and symmetric vibrations of P═O groups, respectively) (Fig. 4C and D). In the A2780 cells exposed to CDs@RuCN, the asymmetric P═O band is shifted toward higher wavenumbers, and a decrease of the same band intensity for about 10% is observed upon illumination compared to the results collected in the dark. Although illumination of the N-CDs@RuCN treated cells did not lead to a shift in the wavenumbers, it increased the intensity of the bands corresponding to the P═O vibrations (~1240 cm^{-1} and 1080 cm^{-1}) by about 30%.

In the case of CAL72 cells, the phosphate band is also changed (Fig. 3D). The band at ~1240 cm^{-1} was shifted towards higher wavenumbers when the cells were treated with both CDs@RuCN and N-CDs@RuCN (red *vs* blue and orange *vs* green line, respectively, Cf.

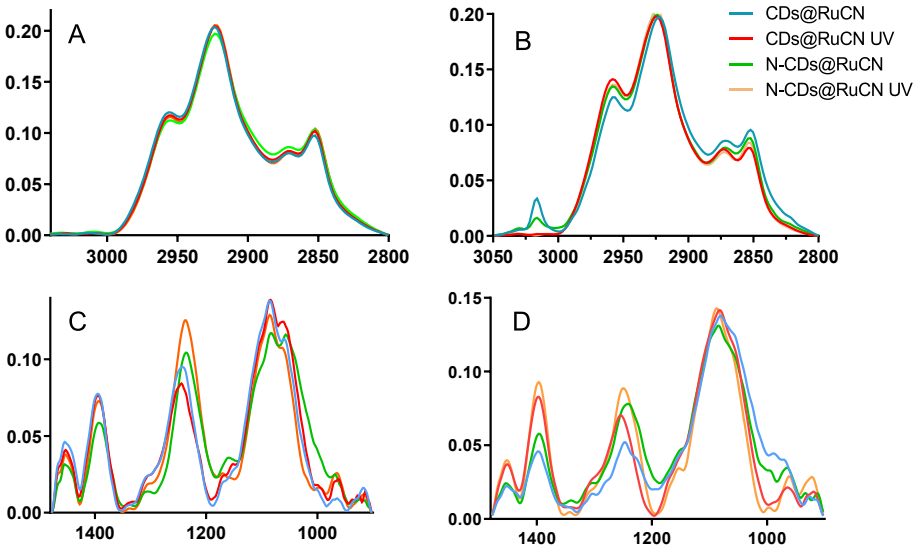

Fig. 4. SR-FTIR spectra of the lipid region (**A,B**) and nucleic acid (**C,D**) regions of A2780 (**A,C**) and CAL72 cells (**B,D**) treated with CDs@RuCN and N-CD@RuCN. Blue lines in the spectra represent the cells treated with CDs@RuCN, and red are the cells treated with CDs@RuCN and illuminated. The treatment with N-CDs@RuCN is represented by the green lines in both spectra, whereas the same treatment upon illumination is given in orange.

Fig. 4). Moreover, in both cases, the intensity of this band increased, implying the changes in the NA structure, especially in DNA [49]. The band's intensity at ~1240 cm^{-1} increased by about 20% when CAL72 was treated with CDs@RuCN (Fig. 4D), and by 30% after its treatment with the N-CDs@RuCN. These data are consistent with the findings of Havrdova et al., who found that the negatively charged CDs entered the cell nucleus to a lesser extent than those with positively charged functional groups, which interact better with DNA [50]. They also reported that negatively charged CDs induce oxidative stress in cells to a higher degree, which is not a light-triggered event. However, we can speculate that in our case, the level of oxidative stress induced by CDs and N-CDs is not sufficient to result in increased cytotoxicity (Fig. 1), but it can promote structural changes in biomolecules.

PCA scores (Figs. S4C and D) also confirm the significance of the different light-induced effects and show a grouping pattern of non-illuminated *vs* illuminated cells, especially in the case of CAL72 cells. The interactions of CDs with NAs are established since CDs have been used for the sensing of NAs [51]. Therefore, their interactions with NAs are also expected in the cellular milieu. Nevertheless, the mechanism of NAs' structural changes upon their interaction with CDs@RuCN and N-CDs@RuCN and light needs to be elucidated. It has been assumed that the interactions of N-CDs with $–NH_2$ group with acidic NAs is electrostatic. In some instances, these interactions can result in the change of the conformation of NAs [52]. As seen in the SR-FTIR spectra and discussed above, these interactions are augmented by light. Additionally, this effect might result from the light-triggered events catalyzed by CDs alone, but also light-induced RuCN isomerization and intercalation into DNA might play a role, as demonstrated for Ru-complexes with polypyridyl ligands [53]. Cardin and co-workers have also documented a photoinduced Ru-complex binding to plasmids DNA [54]. Indeed, various Ru-compounds were found to enter living cells and accumulate in the nucleus (among other organelles) [55]. They could directly damage nuclear DNA utilizing the Ru-compounds' metal-ligand charge transfer "light-switch" property.

The DNA damage mechanism could vary, ranging from the ROS formation and oxidation of guanine [56,57] to photo adduct formation where Ru-complex ligand dissociates upon irradiation followed by the coordination of the resulting Ru-fragment to DNA [13,14]. Some of these fragments might even successfully induce DNA photocleavage [58, 59]. The PC loadings' analysis of the A2780 cells (Fig. S4A) confirms that the most expressed differences in PC1 are observed at the bands ~1020 cm^{-1} and in PC2 at ~1220 and 1010 cm^{-1}. In the case of CAL72, the loading for PC1 (Fig. S4B) shows the most differences in the spectra at ~1220 cm^{-1} and 1010 cm^{-1}. Besides bands at ~1020 cm^{-1} (glycogen) and ~1059 cm^{-1} (carbohydrates) [59], the bands at ~1010 and ~1089 cm^{-1} are in a direct correlation with the Z-form of DNA, which could appear more expressed than the *B*-form after the epigenetic effect of acetylation of histones [60]. Besides, an increase of band at ~1089 cm^{-1} in UV illuminated samples was observed compared to non-illuminated analogues after cell's treatments (Fig. 4D), which could correspond to the Z form/conformation of DNA. Possible transformation of the B form to the Z-DNA form caused by the NPs and UV treatments could finally lead to cell apoptosis. The shift of the position of corresponding NA-related bands is caused by light illumination. The vibrational study of the photosensitizing effect of *hypocrellin* A on HeLa cells, cervical cancer [60], indicates the changes in IR absorption of DNA upon PDT, which imply the apoptotic events in the cells. The systems tested as PS in the present study induce significant changes of NA-related bands in CAL72 compared to unilluminated analogues (Fig. S4D), which is in accordance with the decreased metabolic activity of CAL72 cells line when compared illuminated with unilluminated treatments with NPs (Fig. 1).

5. Conclusions

In conclusion, the results presented in this manuscript are, to our best knowledge, one of the rare detailed reports of intracellular biochemical changes that occur upon the illumination of the CDs-treated cells. We describe the effects attributable exclusively to light stimulation and are selective for the CDs@RuCN and N-CDs@RuCN. Changes in the structure and conformation are observed in three major classes of biomolecules, and a summary of the most pronounced changes is given in Table 3. Our results imply intermediate intracellular events related to an increased ROS production that occur upon light illumination in the presence of pristine and N-modified CDs. These events are different and dependent on the CDs' surface and lead to structural/conformational changes in lipids, proteins, and nucleic acids. Detected changes can be attributed to the vibrational energies and oscillator stress of CDs/RuCN or N-CDs/RuCN combination, as well as to different protein expression in two cell lines. Proteins that are a part of two signalling pathways in the A2780 cells (Wnt) and PI3–K/Akt in the CAL72 cells are identified as potential targets for PDT with CD@RuCN or N-CDs/RuCN. While major

Table 3
Summary of the most pronounced changes in cancer cells biomolecules after indicated treatment conditions.

A2780	**Proteins**-Wnt/β-catenin signalling pathway	**Lipids**	**Nucleic acids**
CDs@RuCN			
CDs@RuCN UV	Change in alpha-helix and random coil structure Target protein: CXXC4		
N-CDs@RuCN	Change in carbonyl and carboxyl groups		
N-CDs@RuCN UV	Change in alpha-helix and random coil structure Target protein: CXXC4		
CAL72	**Proteins**-PI3K/Akt signalling pathway	**Lipids**	**Nucleic acids**
CDs@RuCN	aggregated β-sheet structures; Target proteins: MET, CDK6, FGF1, FN1, ITGA2, ITGA4, IL7R, NGF, PRKCA, THEM4 and THBS2		
CDs@RuCN UV		Reduction in the concentration of unsaturated C═C bonds, higher peroxidation activity (CH_2/CH_3 ratio)	Possible transformation of the B form to the Z-DNA
N-CDs@RuCN			
N-CDs@RuCN UV		Reduction in the concentration of unsaturated C=C bonds, higher peroxidation activity (CH_2/CH_3 ratio)	Possible transformation of the B form to the Z-DNA

changes in ovarian cancer cells are observed in the proteins upon light illumination, the most pronounced changes associated with the effect of light in osteosarcoma cells are observed in lipids and nucleic acids. Therefore, we can speculate that our results can represent a base for selectivity in cancer therapy.

Author contributions

M. Nešić- experimental design, data collection, analysis, interpretation and manuscript draft preparation; T. Dučić- SR-FTIR spectroscopy measurements and data collection, analysis and interpretation; M. Gonçalves- cell preparation; M. Algarra- experimental design and review; M. Stepić- illumination experiments, review and editing of the manuscript; J. Soto- computational DFT calculations; B. Gemović- bioinformatics analysis; T.J. Bandosz- revision of the scientific content of the manuscript; M. Petković- experimental design, data collection, analysis and manuscript review.

Declaration of competing interest

The authors declare that they have no known competing financial interests or personal relationships that could have appeared to influence the work reported in this paper.

Acknowledgements

MP, MN and MA thank to MIRAS Beamline at ALBA Synchrotron for their financial support (experiment Nr. 2019093770). This work was also supported by the Ministry of Education, Science and Technological Development of the Republic of Serbia (grant 451-03-68/2020-14/200017), FCT- (CQM Base Fund - UIDB/00674/2020, and Programmatic Fund - UIDP/00674/2020), Madeira 14–20 Program (project PROEQUIPRAM-Reforço do Investimentoem Equipamentos e Infrastructures Científcasna RAM-M1420-01-0145-FEDER-000008) and by ARDITI-Agência Regional para o Desenvolvimento da Investigação Tecnologia e Inovação through the ARDITI-CQM/2018/007-PDG (Fellowship Grant to MG), project M1420-01-0145-FEDER-000005-CQM+ (Madeira 14–20). MA thanks the Ministerio de Ciencia, Innovación y Universidades, Spain (RTI2018-099668-BC22 project). JS thanks Junta de Andalucía and FEDER founds (projects UMA18-FEDER-JA-049 and P18-RT-4592). JS thanks Larrosa and D. Guerrero for the technical support in running the calculations and the SCBI (Supercomputer and Bioinformatics) of the Univ. Málaga for computer and software resources.

Appendix A. Supplementary data

Supplementary data to this article can be found online at https://doi.org/10.1016/j.cbi.2022.109950.

References

[1] H. He, X. Zheng, S. Liu, M. Zheng, Z. Xie, Y. Wang, M. Yu, X. Shuai, Diketopyrrolopyrrole-based carbon dots for photodynamic therapy, Nanoscale 10 (2018) 10991–10998, https://doi.org/10.1039/C8NR02643B.
[2] M. Lan, L. Guo, S. Zhao, Z. Zhang, Q. Jia, L. Yan, J. Xia, H. Zhang, P. Wang, W. Zhang, Carbon dots as multifunctional phototheranostic agents for photoacoustic/fluorescence imaging and photothermal/photodynamic synergistic cancer therapy, Adv. Ther. 1 (2018) 1800077, https://doi.org/10.1002/adtp.201800077.
[3] P.-C. Hsu, P.-C. Chen, C.-M. Ou, H.-Y. Chang, H.-T. Chang, Extremely high inhibition activity of photoluminescent carbon nanodots toward cancer cells, J. Mater. Chem. B. 1 (2013) 1774, https://doi.org/10.1039/c3tb00545c.
[4] C.-L. Li, C.-M. Ou, C.-C. Huang, W.-C. Wu, Y.-P. Chen, T.-E. Lin, L.-C. Ho, C.-W. Wang, C.-C. Shih, H.-C. Zhou, Y.-C. Lee, W.-F. Tzeng, T.-J. Chiou, S.-T. Chu, J. Cang, H.-T. Chang, Carbon dots prepared from ginger exhibiting efficient inhibition of human hepatocellular carcinoma cells, J. Mater. Chem. B. 2 (2014) 4564, https://doi.org/10.1039/c4tb00216d.
[5] B.B. Campos, C. Abellán, M. Zougagh, J. Jimenez-Jimenez, E. Rodríguez-Castellón, J.C.G. Esteves da Silva, A. Ríos, M. Algarra, Fluorescent chemosensor for pyridine based on N-doped carbon dots, J. Colloid Interface Sci. 458 (2015) 209–216, https://doi.org/10.1016/j.jcis.2015.07.053.
[6] Y. Tang, J. Hu, A.H. Elmenoufy, X. Yang, Highly efficient FRET system capable of deep photodynamic therapy established on X-ray excited mesoporous LaF_3 : Tb scintillating nanoparticles, ACS Appl. Mater. Interfaces 7 (2015) 12261–12269, https://doi.org/10.1021/acsami.5b03067.
[7] T. Kong, L. Hao, Y. Wei, X. Cai, B. Zhu, Doxorubicin conjugated carbon dots as a drug delivery system for human breast cancer therapy, Cell Prolif 51 (2018), e12488, https://doi.org/10.1111/cpr.12488.
[8] J. Pardo, Z. Peng, R. Leblanc, Cancer targeting and drug delivery using carbon-based quantum dots and nanotubes, Molecules 23 (2018) 378, https://doi.org/10.3390/molecules23020378.
[9] D. Rosenblum, N. Joshi, W. Tao, J.M. Karp, D. Peer, Progress and challenges towards targeted delivery of cancer therapeutics, Nat. Commun. 9 (2018) 1410, https://doi.org/10.1038/s41467-018-03705-y.
[10] P. Pierrat, R. Wang, D. Kereselidze, M. Lux, P. Didier, A. Kichler, F. Pons, L. Lebeau, Efficient in vitro and in vivo pulmonary delivery of nucleic acid by carbon dot-based nanocarriers, Biomaterials 51 (2015) 290–302, https://doi.org/10.1016/j.biomaterials.2015.02.017.
[11] X.T. Zheng, A. Ananthanarayanan, K.Q. Luo, P. Chen, Glowing graphene quantum dots and carbon dots: properties, syntheses, and biological applications, Small 11 (2015) 1620–1636, https://doi.org/10.1002/smll.201402648.
[12] Y.K. Jung, E. Shin, B.-S. Kim, Cell nucleus-targeting zwitterionic carbon dots, Sci. Rep. 5 (2015) 18807, https://doi.org/10.1038/srep18807.
[13] J.D. Knoll, C. Turro, Control and utilization of ruthenium and rhodium metal complex excited states for photoactivated cancer therapy, Coord. Chem. Rev. 282–283 (2015) 110–126, https://doi.org/10.1016/j.ccr.2014.05.018.
[14] E. Wachter, D.K. Heidary, B.S. Howerton, S. Parkin, E.C. Glazer, Light-activated ruthenium complexes photobind DNA and are cytotoxic in the photodynamic therapy window, Chem. Commun. 48 (2012) 9649, https://doi.org/10.1039/c2cc33359g.
[15] S. Chio-Srichan, M. Réfrégiers, F. Jamme, S. Kascakova, V. Rouam, P. Dumas, Photosensitizer effects on cancerous cells: a combined study using synchrotron infrared and fluorescence microscopies, Biochim. Biophys. Acta Gen. Subj. 1780 (2008) 854–860, https://doi.org/10.1016/j.bbagen.2008.02.004.
[16] M. Gouveia, J. Figueira, M. Jardim, R. Castro, H. Tomás, K. Rissanen, J. Rodrigues, Poly(alkylidenimine) dendrimers functionalized with the organometallic moiety $[Ru(\eta5\text{-}C_5H_5)(PPh_3)_2]^+$ as promising drugs against cisplatin-resistant cancer cells and human mesenchymal stem cells, Molecules 23 (2018) 1471, https://doi.org/10.3390/molecules23061471.
[17] M. Algarra, B.B. Campos, K. Radotić, D. Mutavdžić, T. Bandosz, J. Jiménez-Jiménez, E. Rodriguez-Castellón, J.C.G. Esteves da Silva, Luminescent carbon nanoparticles: effects of chemical functionalization, and evaluation of Ag+ sensing

properties, J. Mater. Chem. A. 2 (2014) 8342, https://doi.org/10.1039/c4ta00264d.
[18] D. Houdová, J. Soto, R. Castro, J. Rodrigues, M.S. Pino-González, M. Petković, T. J. Bandosz, M. Algarra, Chemically heterogeneous carbon dots enhanced cholesterol detection by MALDI TOF mass spectrometry, J. Colloid Interface Sci. 591 (2021) 373–383, https://doi.org/10.1016/j.jcis.2021.02.004.
[19] M. Louleb, L. Latrous, Á. Ríos, M. Zougagh, E. Rodríguez-Castellón, M. Algarra, J. Soto, Detection of dopamine in human fluids using N-doped carbon dots, ACS Appl. Nano Mater. 3 (2020) 8004–8011, https://doi.org/10.1021/acsanm.0c01461.
[20] I. Yousef, L. Ribó, A. Crisol, I. Šics, G. Ellis, T. Ducic, M. Kreuzer, N. Benseny-Cases, M. Quispe, P. Dumas, S. Lefrançois, T. Moreno, G. García, S. Ferrer, J. Nicolas, M.A. G. Aranda, Miras: The infrared synchrotron radiation beamline at ALBA, Synchrotron Radiat. News 30 (2017) 4–6, https://doi.org/10.1080/08940886.2017.1338410.
[21] M.D. Nešić, T. Dučić, X. Liang, M. Algarra, L. Mi, L. Korićanac, J. Žakula, T.J. Kop, M.S. Bjelaković, A. Mitrović, G.D. Gojgić Cvijović, M. Stepić, M. Petković, SR-FTIR spectro-microscopic interaction study of biochemical changes in HeLa cells induced by Levan-C60, Pullulan-C60, and their cholesterol-derivatives, Int. J. Biol. Macromol. 165 (2020) 2541–2549, https://doi.org/10.1016/j.ijbiomac.2020.10.141.
[22] M. Toplak, G. Birarda, S. Read, C. Sandt, S.M. Rosendahl, L. Vaccari, J. Demšar, F. Borondics, Infrared orange: connecting hyperspectral data with machine learning, Synchrotron Radiat. News 30 (2017) 40–45, https://doi.org/10.1080/08940886.2017.1338424.
[23] I. Papatheodorou, P. Moreno, J. Manning, A.M.-P. Fuentes, N. George, S. Fexova, N.A. Fonseca, A. Füllgrabe, M. Green, N. Huang, L. Huerta, H. Iqbal, M. Jianu, S. Mohammed, L. Zhao, A.F. Jarnuczak, S. Jupp, J. Marioni, K. Meyer, R. Petryszak, C.A. Prada Medina, C. Talavera-López, S. Teichmann, J.A. Vizcaino, A. Brazma, Expression Atlas update: from tissues to single cells, Nucleic Acids Res. (2019) gkz947, https://doi.org/10.1093/nar/gkz947.
[24] D.W. Huang, B.T. Sherman, R.A. Lempicki, Systematic and integrative analysis of large gene lists using DAVID bioinformatics resources, Nat. Protoc. 4 (2009) 44–57, https://doi.org/10.1038/nprot.2008.211.
[25] M. Kanehisa, KEGG: Kyoto Encyclopedia of genes and genomes, Nucleic Acids Res. 28 (2000) 27–30, https://doi.org/10.1093/nar/28.1.27.
[26] R.A. Laskowski, J. Jabłońska, L. Pravda, R.S. Vařeková, J.M. Thornton, PDBsum: structural summaries of PDB entries, Protein Sci. 27 (2018) 129–134, https://doi.org/10.1002/pro.3289.
[27] Y. Zhao, N.E. Schultz, D.G. Truhlar, Design of density functionals by combining the method of constraint satisfaction with parametrization for thermochemistry, thermochemical kinetics, and noncovalent interactions, J. Chem. Theor. Comput. 2 (2006) 364–382, https://doi.org/10.1021/ct0502763.
[28] S. Grimme, J. Antony, S. Ehrlich, H. Krieg, A consistent and accurate *ab initio* parametrization of density functional dispersion correction (DFT-D) for the 94 elements H-Pu, J. Chem. Phys. 132 (2010) 154104, https://doi.org/10.1063/1.3382344.
[29] F. Weigend, Accurate Coulomb-fitting basis sets for H to Rn, Phys. Chem. Chem. Phys. 8 (2006) 1057, https://doi.org/10.1039/b515623h.
[30] N. Nunes, I. Popović, E. Abreu, D. Maciel, J. Rodrigues, J. Soto, M. Algarra, M. Petković, Detection of Ru potential metallodrug in human urine by MALDI-TOF mass spectrometry: validation and options to enhance the sensitivity, Talanta 222 (2021) 121551, https://doi.org/10.1016/j.talanta.2020.121551.
[31] R. Hussien, B.H. Rihn, H. Eidi, C. Ronzani, O. Joubert, L. Ferrari, O. Vazquez, D. Kaufer, G.A. Brooks, Unique growth pattern of human mammary epithelial cells induced by polymeric nanoparticles, Phys. Rep. 1 (2013), https://doi.org/10.1002/phy2.27.
[32] Y. Jiao, Y. Guo, Y. Fan, R. Wang, X. Li, H. Wu, Z. Meng, X. Yang, Y. Cui, H. Liu, L. Pan, T. Maimaitijuma, J. Zhang, Y. Wang, Y. Cao, T. Zhang, Triggering of apoptosis in osteosarcoma 143B cell line by carbon quantum dots via the mitochondrial apoptotic signal pathway, BioMed Res. Int. (2020) 1–12, https://doi.org/10.1155/2020/2846297, 2020.
[33] J.M. Dąbrowski, Reactive oxygen species in PhotodynamicTherapy: mechanisms of their generation and potentiation, in: Advances in Inorganic Chemistry, Elsevier, 2017, pp. 343–394, https://doi.org/10.1016/bs.adioch.2017.03.002.
[34] S. Salatin, S. Maleki Dizaj, A. Yari Khosroushahi, Effect of the surface modification, size, and shape on cellular uptake of nanoparticles: cellular uptake of nanoparticles, Cell Biol. Int. 39 (2015) 881–890, https://doi.org/10.1002/cbin.10459.
[35] T. Dučić, S. Stamenković, B. Lai, P. Andjus, V. Lučić, Multimodal synchrotron radiation microscopy of intact astrocytes from the hSOD1 G93A rat model of amyotrophic lateral sclerosis, Anal. Chem. 91 (2019) 1460–1471, https://doi.org/10.1021/acs.analchem.8b04273.
[36] Z. Wei, D. Jiao, J. Xu, Using fourier transform infrared spectroscopy to study effects of magnetic field treatment on wheat (*triticumaestivum* L.) seedlings, J. Spectrosc. (2015) 1–6, https://doi.org/10.1155/2015/570190, 2015.
[37] H. Alhazmi, FT-IR spectroscopy for the identification of binding sites and measurements of the binding interactions of important metal ions with bovine Serum Albumin, Sci. Pharm. 87 (2019) 5, https://doi.org/10.3390/scipharm87010005.
[38] Y. Abe, S. Krimm, Normal vibrations of crystalline polyglycine I, Biopolymers 11 (1972) 1817–1839, https://doi.org/10.1002/bip.1972.360110905.
[39] M.J. Baker, J. Trevisan, P. Bassan, R. Bhargava, H.J. Butler, K.M. Dorling, P. R. Fielden, S.W. Fogarty, N.J. Fullwood, K.A. Heys, C. Hughes, P. Lasch, P. L. Martin-Hirsch, B. Obinaju, G.D. Sockalingum, J. Sulé-Suso, R.J. Strong, M. J. Walsh, B.R. Wood, P. Gardner, F.L. Martin, Using Fourier transform IR spectroscopy to analyze biological materials, Nat. Protoc. 9 (2014) 1771–1791, https://doi.org/10.1038/nprot.2014.110.
[40] J. Zhang, X.-H. Yu, Y.-G. Yan, C. Wang, W.-J. Wang, PI3K/Akt signaling in osteosarcoma, Clin. Chim. Acta 444 (2015) 182–192, https://doi.org/10.1016/j.cca.2014.12.041.
[41] S. Jin, R.-P. Pang, J.-N. Shen, G. Huang, J. Wang, J.-G. Zhou, Grifolin induces apoptosis via inhibition of PI3K/AKT signalling pathway in human osteosarcoma cells, Apoptosis 12 (2007) 1317–1326, https://doi.org/10.1007/s10495-007-0062-z.
[42] Z.-J. Meng, N. Wu, Y. Liu, K.-J. Shu, X. Zou, R.-X. Zhang, C.-J. Pi, B.-C. He, Z.-Y. Ke, L. Chen, Z.-L. Deng, L.-J. Yin, Evodiamine inhibits the proliferation of human osteosarcoma cells by blocking PI3K/Akt signaling, Oncol. Rep. 34 (2015) 1388–1396, https://doi.org/10.3892/or.2015.4084.
[43] S. Sirikwanpong, W. Dahlan, S. Ngamukote, S. Sangsuthum, S. Adisakwattana, V. Nopponpunth, T. Himathongkam, The alterations of erythrocyte phospholipids in type 2 diabetes observed after oral high-Fat Meal loading: the FTIR spectroscopic and mass spectrometric studies, J. Clin. Biochem. Nutr. 47 (2010) 111–120, https://doi.org/10.3164/jcbn.10-21.
[44] P. Foroozandeh, A.A. Aziz, Insight into cellular uptake and intracellular trafficking of nanoparticles, Nanoscale Res. Lett. 13 (2018) 339, https://doi.org/10.1186/s11671-018-2728-6.
[45] S. Wu, R. Zhou, H. Chen, J. Zhang, P. Wu, Highly efficient oxygen photosensitization of carbon dots: the role of nitrogen doping, Nanoscale 12 (2020) 5543–5553, https://doi.org/10.1039/C9NR10986B.
[46] M. Kreuzer, S. Stamenković, S. Chen, P. Andjus, T. Dučić, Lipids status and copper in a single astrocyte of the rat model for amyotrophic lateral sclerosis: correlative synchrotron-based X-ray and infrared imaging, J. Biophot. 13 (2020), https://doi.org/10.1002/jbio.202000069.
[47] L. Lilge, Use of ruthenium complexes as photosensitizers in photodynamic therapy, in: W.R. Browne, A.A. Holder, M.A. Lawrence, J.L. Bullock Jr., L. Lilge (Eds.), Ruthenium Complexes, Wiley-VCH VerlagGmbH& Co. KGaA, Weinheim, Germany, 2017, pp. 117–137, https://doi.org/10.1002/9783527695225.ch6.
[48] N. Kanwa, K. M, A. Chakraborty, Discriminatory interaction behavior of lipid vesicles toward diversely emissive carbon dots synthesized from ortho, meta, and para isomeric carbon precursors, Langmuir 36 (2020) 10628–10637, https://doi.org/10.1021/acs.langmuir.0c02207.
[49] M. Havrdova, K. Hola, J. Skopalik, K. Tomankova, M. Petr, K. Cepe, K. Polakova, J. Tucek, A.B. Bourlinos, R. Zboril, Toxicity of carbon dots – effect of surface functionalization on the cell viability, reactive oxygen species generation and cell cycle, Carbon 99 (2016) 238–248, https://doi.org/10.1016/j.carbon.2015.12.027.
[50] A.H. Loo, Z. Sofer, D. Bouša, P. Ulbrich, A. Bonanni, M. Pumera, Carboxylic carbon quantum dots as a fluorescent sensing platform for DNA detection, ACS Appl. Mater. Interfaces 8 (2016) 1951–1957, https://doi.org/10.1021/acsami.5b10160.
[51] H. Sun, J. Ren, X. Qu, Carbon nanomaterials and DNA: from molecular recognition to applications, Acc. Chem. Res. 49 (2016) 461–470, https://doi.org/10.1021/acs.accounts.5b00515.
[52] C.J. Cardin, J.M. Kelly, S.J. Quinn, Photochemically active DNA-intercalating ruthenium and related complexes – insights by combining crystallography and transient spectroscopy, Chem. Sci. 8 (2017) 4705–4723, https://doi.org/10.1039/C7SC01070B.
[53] V.H.S. van Rixel, B. Siewert, S.L. Hopkins, S.H.C. Askes, A. Busemann, M.A. Siegler, S. Bonnet, Green light-induced apoptosis in cancer cells by a tetrapyridyl ruthenium prodrug offering two trans coordination sites, Chem. Sci. 7 (2016) 4922–4929, https://doi.org/10.1039/C6SC00167J.
[54] L. Zeng, P. Gupta, Y. Chen, E. Wang, L. Ji, H. Chao, Z.-S. Chen, The development of anticancer ruthenium(ii) complexes: from single molecule compounds to nanomaterials, Chem. Soc. Rev. 46 (2017) 5771–5804, https://doi.org/10.1039/C7CS00195A.
[55] B. Elias, C. Creely, G.W. Doorley, M.M. Feeney, C. Moucheron, A. Kirsch-DeMesmaeker, J. Dyer, D.C. Grills, M.W. George, P. Matousek, A.W. Parker, M. Towrie, J.M. Kelly, Photooxidation of guanine by a ruthenium dipyridophenazine complex intercalated in a double-stranded polynucleotide monitored directly by picosecond visible and infrared transient absorption spectroscopy, Chem. Eur J. 14 (2008) 369–375, https://doi.org/10.1002/chem.200700564.
[56] L. Herman, S. Ghosh, E. Defrancq, A.K.-D. Mesmaekera, Ru(II) complexes and light: molecular tools for biomolecules, J. Phys. Org. Chem. 21 (2008) 670–681, https://doi.org/10.1002/poc.1355.
[57] S.M. Cloonan, R.B.P. Elmes, M. Erby, S.A. Bright, F.E. Poynton, D.E. Nolan, S. J. Quinn, T. Gunnlaugsson, D.C. Williams, Detailed biological profiling of a photoactivated and apoptosis inducing pdppz ruthenium (II) polypyridyl complex in cancer cells, J. Med. Chem. 58 (2015) 4494–4505, https://doi.org/10.1021/acs.jmedchem.5b00451.
[58] G.J. Ryan, S. Quinn, T. Gunnlaugsson, Highly effective DNA photocleavage by novel "rigid" Ru $(bpy)_3$ -4-nitro- and -4-amino-1,8-naphthalimide conjugates, Inorg. Chem. 47 (2008) 401–403, https://doi.org/10.1021/ic700967y.
[59] K. Malek, B.R. Wood, K.R. Bambery, FTIR imaging of tissues: techniques and methods of analysis, in: M. Baranska (Ed.), Optical Spectroscopy and Computational Methods in Biology and Medicine, Springer Netherlands, Dordrecht, 2014, pp. 419–473, https://doi.org/10.1007/978-94-007-7832-0_15.
[60] J. Zhang, E.-H. Cao, J.-F. Li, T.-C. Zhang, W.-J. Ma, Photodynamic effects of hypocrellin A on three human malignant cell lines by inducing apoptotic cell death, J. Photochem. Photobiol. B Biol. 43 (1998) 106–111, https://doi.org/10.1016/S1011-1344(98)00092-X.